SHEAR STRENGTH CHARACTERISTICS OF SHIRAZ UNSATURATED SILTY CLAY[*]

A. FAZELI, G. HABIBAGAHI[**] AND A. GHAHRAMANI

Dept. of Civil Engineering, Shiraz University, Shiraz, I. R. of Iran
Email: habibg@shirazu.ac.ir

Abstract– This paper provides the results of ten triaxial tests which were carried out to study the unsaturated shear strength characteristics of Shiraz silty clay soil. The soil tested was reconstituted using static compaction. Consolidated drained (CD) triaxial tests were performed on both saturated and unsaturated samples at various net confining pressures and matric suctions. Digital image processing technique is used to measure the total volume change of the specimens. The accuracy of this technique is discussed by comparing the results with the volume change of the saturated tests determined from the conventional method. The volume change is also used to determine the change in sample diameter which is used to correct the deviatoric stress accordingly. Shear strength parameters c', ϕ' and χ are determined from the test results and dependence of parameter χ on soil suction is studied and compared with the available relationships in literature. Furthermore, it is shown that the shear strength of both saturated and unsaturated soil specimens fall on a single line in the effective stress space. Therefore, applicability of the effective stress principle for the shear strength of unsaturated Shiraz silty clay is clearly validated.

1. INTRODUCTION

In arid and semi-arid regions the ground water table is located well below the ground surface. Moreover, most embankments, natural slopes, landfill liners and retaining wall backfills are constructed on or with unsaturated soils. Hence, the study of unsaturated soil behavior is very important for a better design and analysis. Research in this area dates back to the 1950's [1, 2]. Two main characteristics of mechanical behavior of unsaturated soils are their shear strength and volume change. Constitutive models have been presented to describe the mechanical behavior of these soils [3, 4]. Triaxial shear, direct shear, simple shear and consolidation tests are among the tests used to calibrate these models [5-7]. Also, empirical relationships between some characteristics of the water retention curve (WRC) and the contribution of suction to shear strength have been proposed [8-11]. WRC shows the variation of gravimetric water content, volumetric water content or degree of saturation versus matric suction. The above mentioned empirical relationships require shear strength parameters obtained from tests on saturated soil specimens as well as pressure plate test results (WRC) which are simpler and cheaper, relative to other sophisticated tests on unsaturated soils.

There are currently two different approaches for modeling the shear strength of unsaturated soils, namely, effective stress approach and approach based on two independent state variables. Nuth and Laloui [12] showed that there is no need for the two stress variables to be independent. Based on the effective stress principle, Bishop [2] extended the Mohr-Coulomb failure criteria from saturated to unsaturated state, given by:

$$\tau_f = c' + [(\sigma_n - u_a) + \chi(u_a - u_w)]\tan\phi' \tag{1}$$

Where:

$\tau_f =$ shear strength of unsaturated soil

$c' =$ effective cohesion

$\phi' =$ effective friction angle

$(\sigma_n - u_a) =$ net normal stress

$(u_a - u_w) =$ matric suction

$\chi =$ effective stress parameter

The effective stress parameter χ is related to the degree of saturation and varies between 0 and 1 corresponding to dry and saturated states, respectively. More recently, Nuth and Laloui [12] presented two categories for the Bishop effective stress depending on the dependence of χ parameter on suction or degree of saturation.

Fredlund et al. [13] proposed an equation based on two independent state variables, that is:

$$\tau_f = c' + (\sigma_n - u_a)\tan\phi' + (u_a - u_w)\tan\phi^b \tag{2}$$

In the three dimensional space, $\{\tau_f\_(u_a - u_w)\_(\sigma_n - u_a)\}$, ϕ^b is slope of failure surface in $\{\tau_f\_(u_a - u_w)\}$ plane. Fredlund et al. [13] assumed ϕ^b and ϕ' as constant parameters but it was shown later that this assumption is not realistic. For suctions smaller than the air entry value, ϕ^b is equal to ϕ' but decreases with an increase in matric suction [14]. For matric suctions up to 600 kPa, ϕ' is nearly constant [9].

Unsaturated shear strength in both Eqs. (1) and (2) have two separate terms: a saturated shear strength term, $\tau_{sat} = c' + (\sigma_n - u_a)\tan\phi'$ assuming $u_a = u_w$, and the contribution to shear strength from matric suction, $\tau_{unsat} = \chi(u_a - u_w)\tan\phi'$ in Eq. (1) and $\tau_{unsat} = (u_a - u_w)\tan\phi_b$ in Eq. (2). There are also some empirical procedures to obtain τ_{unsat}. These are listed below: [8, 15, 10, 11, 16]

$$\tau_{unsat} = (u_a - u_w)\theta\tan\phi' \tag{3}$$

$$\begin{cases} \tau_{unsat} = (u_a - u_w)\Theta^\kappa\tan\phi' \\ \Theta = \dfrac{\theta}{\theta_s} \text{ for } \theta \le \theta_s \\ \kappa = -0.0016 I_p^2 + 0.0975 I_p + 1 \end{cases} \tag{4}$$

$$\begin{cases} \tau_{unsat} = (u_a - u_w)\chi\tan\phi' \\ \chi = \left[\dfrac{(u_a - u_w)}{(u_a - u_w)_b}\right]^{-0.55} \text{ for } (u_a - u_w) \ge (u_a - u_w)_b \end{cases} \tag{5}$$

$$\begin{cases} \tau_{unsat} = (u_a - u_w)_b^{1-\varsigma}(u_a - u_w)^\varsigma\tan\phi' \\ \varsigma = D_s - 2 \end{cases} \tag{6}$$

$$\tau_{unsat} = \tan\phi'((u_a - u_w)_b + P_{at})\ln\left[\dfrac{(u_a - u_w) + P_{at}}{P_{at}}\right] \tag{7}$$

Where:

$\theta =$ volumetric water content

I_P = plasticity index

θ_s = saturated volumetric water content

Θ = normalized volumetric water content

$(u_a - u_w)_b$ = air entry value of soil

ς = fractal dimension

D_s = pore distribution factor

P_{at} = atmospheric pressure (101.3kpa)

The shear strength contribution from the matric suction can also be obtained by performing triaxial tests on saturated and unsaturated samples and using Eq. (8).

$$\tau_{unsat} = \tau_f - \tau_{sat} \tag{8}$$

Axial stress in triaxial tests must be corrected to account for the change in sample diameter. However, volume change or radial strain measurement of the unsaturated soil samples in the triaxial test is not an easy task. Lateral strain gauges [17], noncontacting transducers [18,19] or cell liquid volume measurement using double-walled triaxial cell [20] can be used to measure the radial strain or volume change. Most recently, image processing (IP) using digital cameras has proved to be a suitable technique. This method has some advantages relative to other methods. Firstly, lateral strains can be measured continuously along the sample height, there is no need to modify the triaxial cell, and homogeneity and axisymmetric behavior of the sample can be detected. Application of IP method in triaxial tests on unsaturated specimens has been discussed by different researchers [21-26].

The main aim of this research is to obtain shear strength parameters of Shiraz silty clay in the unsaturated state. For this purpose 10 saturated and unsaturated CD triaxial tests were performed following various stress paths. Pressure plate tests were also performed to obtain the soil water characteristic curve in order to compare the results with the previously mentioned empirical procedures. The test procedure and test results are described in the following sections of this paper.

2. MATERIAL AND TEST PROCEDURE

a) Soil properties

The soil used in this research was Shiraz silty clay. Shiraz is located in a semi-arid region of Iran. Physical and mechanical properties of this soil are shown in Table 1. Pressure plate test was also performed to obtain the WRC of the soil. This test was performed on samples compacted statically following the procedure suggested by ASTM D-6836 [27]. The sample characteristics and preparation procedure were the same as the triaxial test samples presented in the next section. The WRC for this soil is shown in Fig. 1. Based on the test results, the air entry value of the soil was determined to be about 40 kPa.

Table 1. Basic soil properties

LL	PL	PI	Sand	Silt	Clay	Gs	Classification	ω_{opt}	$\gamma_{d,\max}$	C'	ϕ'
33	21	12	12%	58%	30%	2.70	CL	18%	1.82 Mg/m³	4.3 kPa	30.4

b) Triaxial test procedure

The air dried soil was passed through a #10 sieve to prevent nonhomogeneity due to coarse particles. The soil was then carefully moistened using distilled water to obtain 21% water content and sealed in a plastic bag for water content equalization for a period of 48 hours. Soil compaction was performed statically in 10 layers. Hence, a special mold having a diameter of 50 mm and a height of 100 mm was

designed for static compaction of the sample. The target dry density was 1.6 Mg/m^3 in this research. Obtaining more homogeneous samples and higher plasticity or flexibility were the reasons for choosing static compaction method [28].
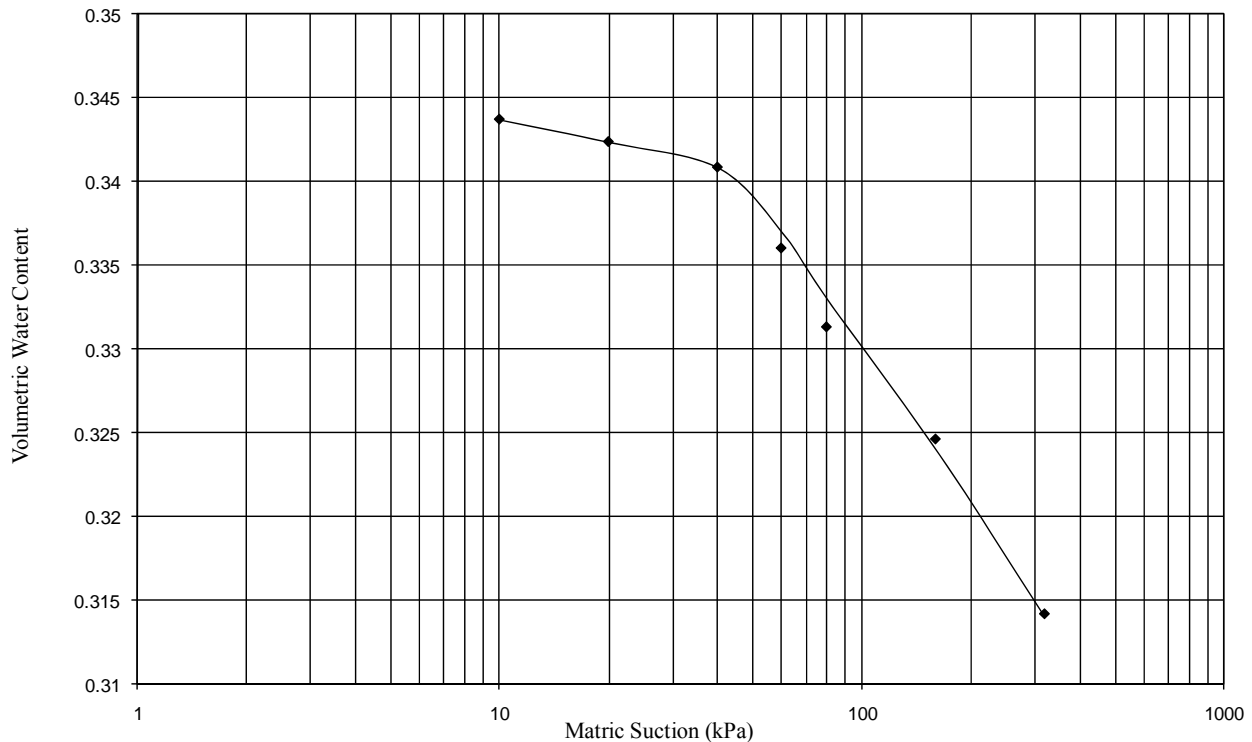

Fig. 1. Water retention curve

The triaxial tests were performed using a Bishop-Wesley hydraulic triaxial cell [29] which was appropriately modified for unsaturated soils. Using this triaxial cell which is shown in Fig. 2 and the TRIAX 4.0 software [30], the triaxial tests may be performed following various stress paths. The air entry value of the ceramic disc which was used in this triaxial cell was about 430 kPa (nominal 3 Bar).

In the first stage, three saturated CD triaxial tests were carried out. The main purpose of these tests was to obtain saturated shear strength parameters and to validate the results of digital image processing technique by comparing the measurement of the net water flow in or out of the soil specimens which is equal to the total volume change in saturated tests. The soil samples were saturated using back pressure until a B-value of 0.98 was achieved. Duration required for saturation was about 3 days. Consolidation was performed in the next stage by increasing the cell pressure. End of primary consolidation stage (t_{100}) was determined by Taylor method. In the final stage, the samples were sheared by increasing the axial strain. The rate of axial strain was fixed at 0.4 mm/hr. End of shearing was assumed when the stress-strain curve leveled off or reached 20% axial strain. Specifications of saturated tests are shown in Table 2.

In the second stage, seven unsaturated CD triaxial tests were performed. The matric suction was kept constant during the shear stage. Hence, the air and water pressures were controlled from the top porous stone and the bottom ceramic disk, respectively [31]. The first part of the test was matric suction equalization. The matric suction was applied by controlling the air and water pressure difference. A rate of change of water specific volume *(1+es)* less than 0.001 per day (about 0.12 cc/day for this research) was considered as the criteria for end of suction equalization [3]. The samples were then consolidated by applying cell pressure increments to arrive at the required value of mean net pressure *(p-u$_a$)*. Finally, the samples were sheared by applying a controlled rate of axial strain. The rate of loading was determined

based on a theoretical method [31]. The rate decreased with increase of matric suction due to the decrease in soil permeability. Time to failure was increased about 1 day for each 10 kPa increase in matric suction. Stress-strain curve leveling off or 20% axial strain was considered as the criterion for failure. Net cell pressure and matric suction were kept constant during shearing. Specifications of unsaturated tests are listed in Table 2. Five tests were performed following the conventional stress path ($\Delta q / \Delta (p - u_a) = 3$) and two other tests were carried out using different stress paths. Two tests, UNSAT1 and UNSAT5, were retested to verify reproducibility of the test results. The results were very close to the main tests.

Table 2. Test specifications

Saturated tests				
Test	$(\sigma_3 - u_w)$	Stress path		
SAT1	50	Conventional		
SAT2	150	Conventional		
SAT3	250	Conventional		
Unsaturated tests				
Test	$(\sigma_3 - u_a)_{initial}$	$(u_a - u_w)$	$(\sigma_3 - u_a)_{failure}$	Stress path
UNSAT1	40	60	40	Conventional
UNSAT2	100	100	100	Conventional
UNSAT3	200	200	200	Conventional
UNSAT4	200	150	200	Conventional
UNSAT5	150	80	53	Constant p=280
UNSAT6	100	130	526	1) q=p
	526	130	366	2) Constant p=920
UNSAT7	160	240	160	Conventional

c) Digital image processing for measurement of total volume change

Two digital cameras (DigiLife DDV60) with 3 Mega pixel resolution were used in this research and connected to a PC through USB ports. Cameras were fixed relative to the triaxial cell using metallic stands as shown in Fig. 2. Two low-watt light sources were connected to the base table for providing uniform lightening of the sample. A dark paper was attached behind the specimen on the cell as a dark background to provide a clear boundary for the specimen. A Windows script was coded to control the cameras and taking pictures automatically at the required time intervals.
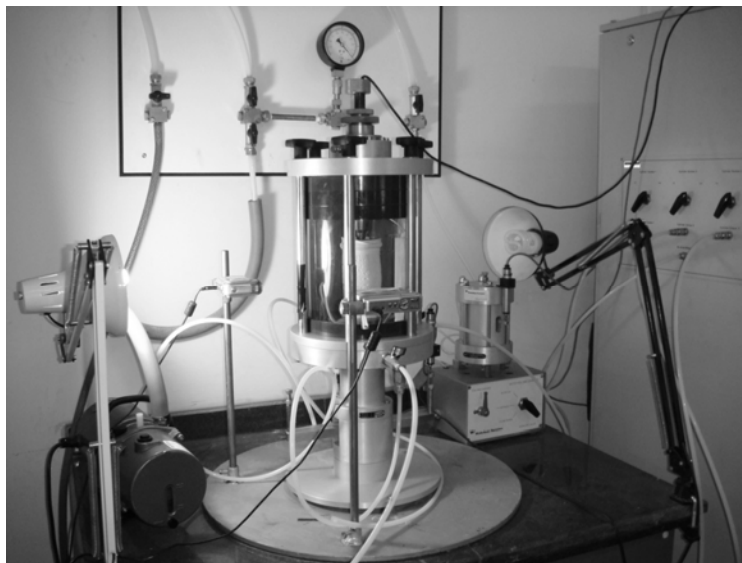

Fig. 2. Bishop-Wesley triaxial cell

The image type was RGB or true-color and information was stored digitally in an m-by-n-by-3 matrix that defines red, green, and blue color components for each individual pixel. The resolution of the images was 2048 by 1536 pixels (Fig. 3a). The images were processed using MATLAB image processing toolbox [32]. Conversion of the images to gray-scale type was the first stage of the image processing (Fig. 3b). MATLAB stores the gray-scale image as a 2D matrix, where each element of the matrix corresponds to one image pixel. The elements in the matrix represent various gray levels, where levels 0 and 255 represent black and white, respectively.

(a)   (b)

(c)   (d)

(e)
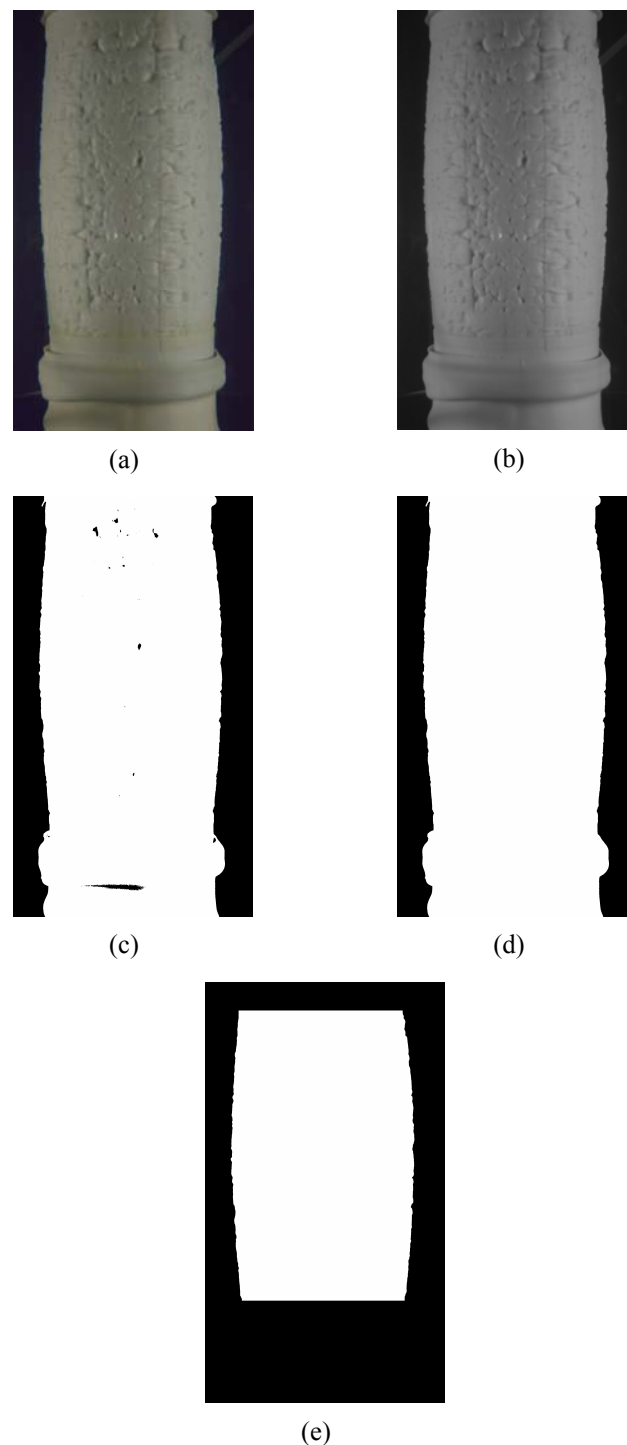
Fig. 3. Different stages of image processing, a- RGB image, b- Gray scale image,
c- Binary image, d- Cleaned image, e- Perspective corrected image

Threshold procedure [25, 26] was used in this research to process the image and separate the specimen from the background. Based on this approach, the gray-scale image is converted to a binary image using a threshold value between 0 and 1 (Fig. 3c). The binary image has a value of 0 (black) for all pixels in the gray-scale image with normalized intensity less than the threshold value and 1 (white) for all other pixels. MATLAB determines the threshold value based on Otsu's method, which chooses the threshold to minimize the intraclass variance of the black and white pixels [33]. In the next stage, the image was cleaned by converting all isolated white or black pixels to black or white, respectively. These isolated pixels were considered as local noise (Fig. 3d). After this stage, the top and bottom boundary of the sample was delineated manually by visual inspection. In this stage, perspective correction was also performed [26]. Due to the perspective effect and the small distance between the sample and the cameras, the top and bottom of the sample are viewed as an ellipse. These ellipses must be erased to obtain an image which shows the orthogonal axis plane of the sample (Fig. 3e).

Finally, the sample height and its diameter in pixels at various heights were obtained from the image as shown in Fig. 3e. Next, these dimensions in pixels must be converted to millimeters. For this purpose a calibration procedure was carried out using 4 metallic cylindrical samples with known dimensions which were installed in a triaxial cell filled with water. Pictures were then taken from the samples by both cameras. Calibration was performed and Eqs. (9) and (10) were obtained between height in pixels and height in millimeters as well as between diameter in pixels and diameter in millimeters, respectively.

$$h^{(mm)} = 0.0553h^{(pixels)} + 2.2923 \tag{9}$$

$$d^{(mm)} = 0.0475d^{(pixels)} + 1.5836 \tag{10}$$

Calibration curves were slightly parabolic but for small variations in height or diameter they may be considered linear as given by Eqs. (9) and (10). The R^2 values were 0.9997 and 0.9993 for the above relationships, respectively.

The digital image processing technique was validated by the volume change results of saturated triaxial tests and also by axial deformation in all tests, which was measured using an LVDT. In saturated triaxial tests, the volume change can be easily measured using as automatic or twin- burette volume change indicator. Figures 4 to 6 show volume change results which were obtained by IP and automatic volume change indicator for the three saturated specimens. The average mean sum square error (MSSE) of volume change measurement by IP for the three tests was 0.12 cc. The average of MSSE of axial deformation measurement by IP for all saturated and unsaturated tests was 0.062 mm. these values correspond to the average error of 5.8% and 3.15% in volumetric strain and axial deformation, respectively.

3. RESULTS AND DISCUSSION

Variation of deviatoric stress (q) versus deviatoric strain (ε_q) for the three saturated specimens is shown in Fig. 7. The deviatoric stress was corrected based on the cross section area variation during the shear stage. In all three tests, the samples reached the critical state. Variation of major principle stress (σ_1) versus minor principle stress (σ_3) is shown in Fig. 8. According to this figure the drained friction angle (ϕ') and the drained cohesion (C') of the soil were determined as 30.4 degrees and 4.3 kPa, respectively.

Figure 9 shows variation of deviatoric stress (q) and volumetric strain (ε_v) versus deviatoric strain (ε_q) for all unsaturated tests. Volumetric strain and shear strength at failure increased with the increase in matric suction and the confining pressure. Based on values of σ_1 and σ_3 at failure and using Eqs. (11) and (12), the χ parameter was calculated for each test as indicated below:

$$\sigma_1' = \sigma_3' \tan^2(45 + \phi'/2) + 2c' \tan(45 + \phi'/2) \tag{11}$$

Where:

$$\sigma_1' = (\sigma_1 - u_a) + \chi(u_a - u_w)$$

$$\sigma_3' = (\sigma_3 - u_a) + \chi(u_a - u_w)$$

Finally:

$$\chi = \frac{(\sigma_1 - u_a) - (\sigma_3 - u_a)\tan^2(45 + \phi'/2) - 2c'\tan(45 + \phi'/2)}{(u_a - u_w)(\tan^2(45 + \phi'/2) - 1)} \tag{12}$$

Figure 10 shows variation of χ versus matric suction. Based on these results, Eq. (13) was considered as a suitable relationship between χ and matric suction.

$$\chi = \left(\frac{(u_a - u_w)}{(u_a - u_w)_b} \right)^m \tag{13}$$
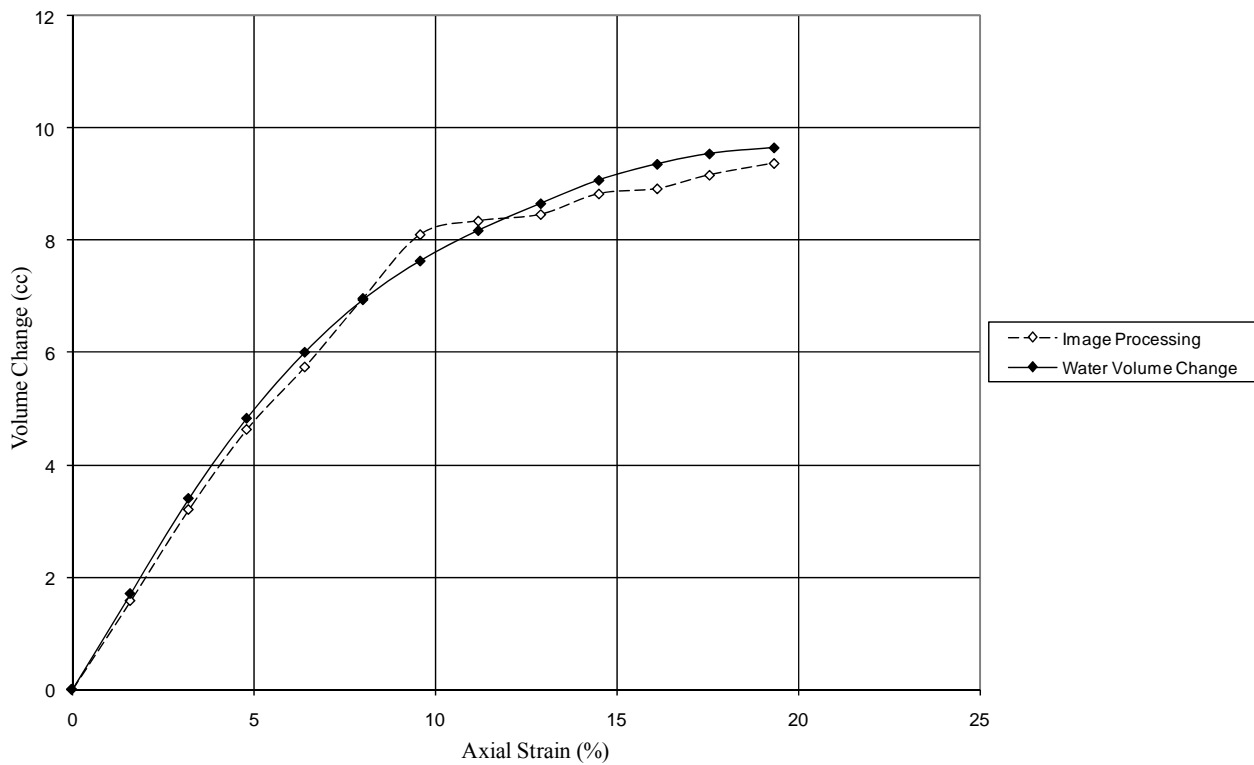
Fig. 4. Variation of volume change versus axial strain for saturated sample (SAT1)

The parameters $(u_a - u_w)_b$ and m obtained from fitting Eq. (13) to the test results were 38 kPa and -0.16, respectively. The predicted χ values calculated using Eq. (5) are also presented in Fig. 10. The power of Eq. (5) was considered as (-0.4) as recommended by Khalili and Khabbaz [10] for clayey soils. The air entry value was considered 38 kPa in Eq. (5). The air entry value estimated based on the curve fitting of Eq. (13) was very close to the air entry value obtained from WRC, 40 kPa. The difference between these values may be attributed to the effect of the confining pressure.

Variation of shear strength contribution from matric suction τ_{unsat} versus matric suction $(u_a$-$u_w)$ is presented in Fig. 11. From this figure, it may be concluded that the results have good agreement with the values predicted using Eq. (7), while Eq. (5) underestimates the shear strength of Shiraz silty clay.
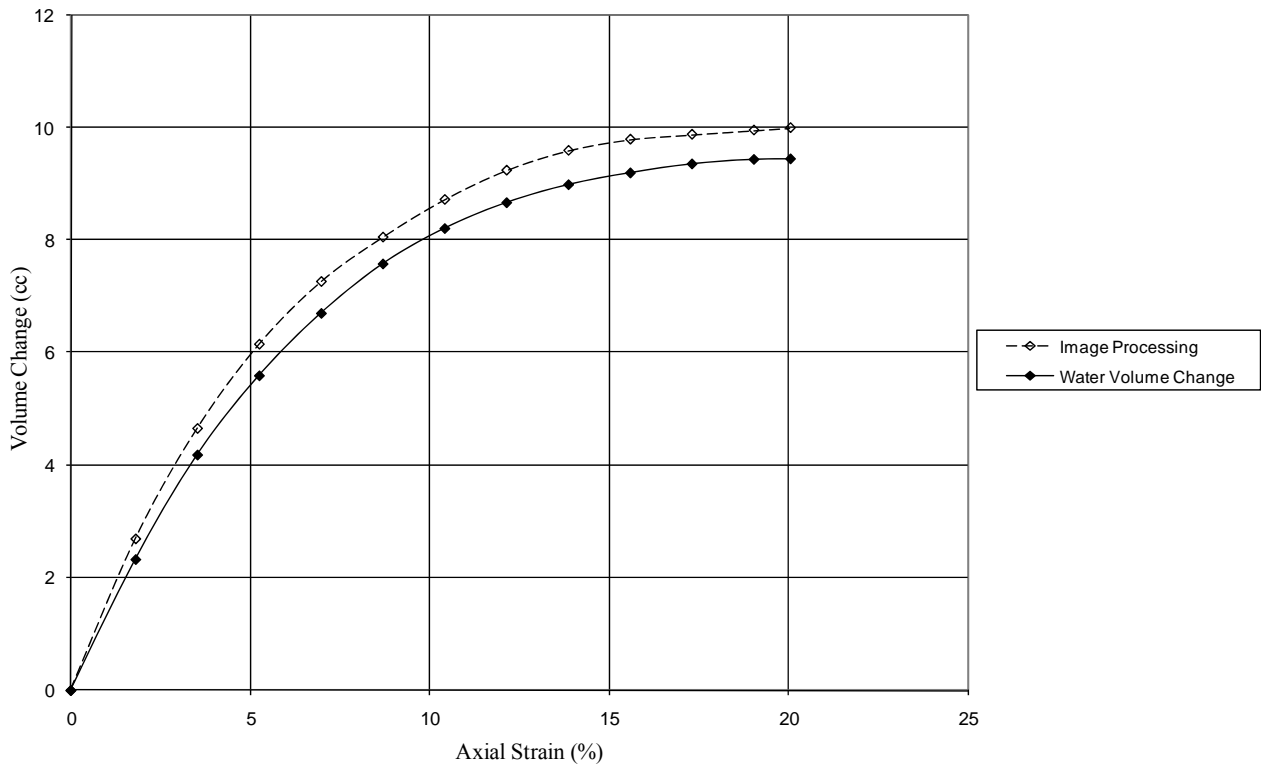
Fig. 5. Variation of volume change versus axial strain for saturated sample (SAT2)
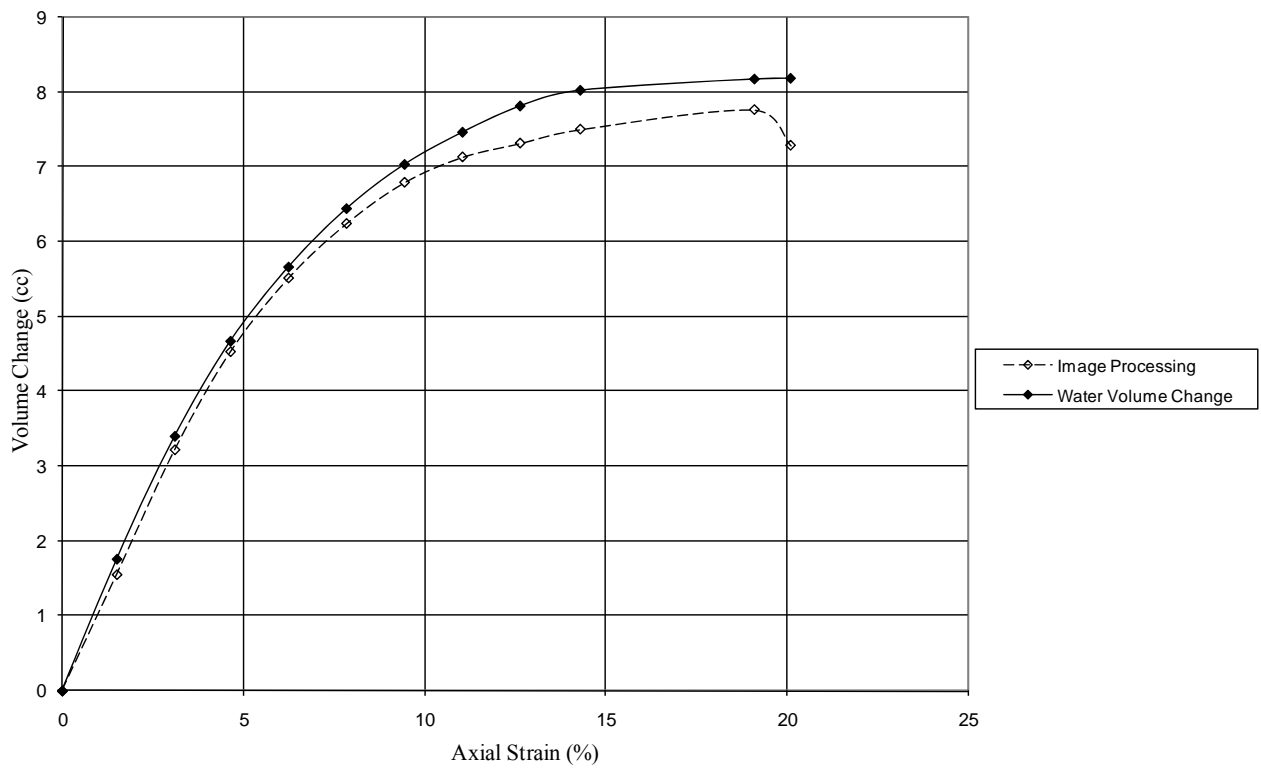

Fig. 6. Variation of volume change versus axial strain for saturated sample (SAT3)

Figure 12 shows variation of deviatoric stress q versus mean effective stress p' for all saturated and unsaturated tests. Mean effective stress was calculated using Eq. (14).

$$p' = (p - u_a) + \chi(u_a - u_w) \tag{14}$$

The unique linear relationship between deviatoric stress and the mean effective stress for all saturated and unsaturated tests, shown in Fig. 12, clearly confirms the validity of the effective stress principle for mechanical modeling of unsaturated soils. Based on this figure, the value of M parameter for the Cam-Clay model can be estimated as 1.2027 for Shiraz silty clay.
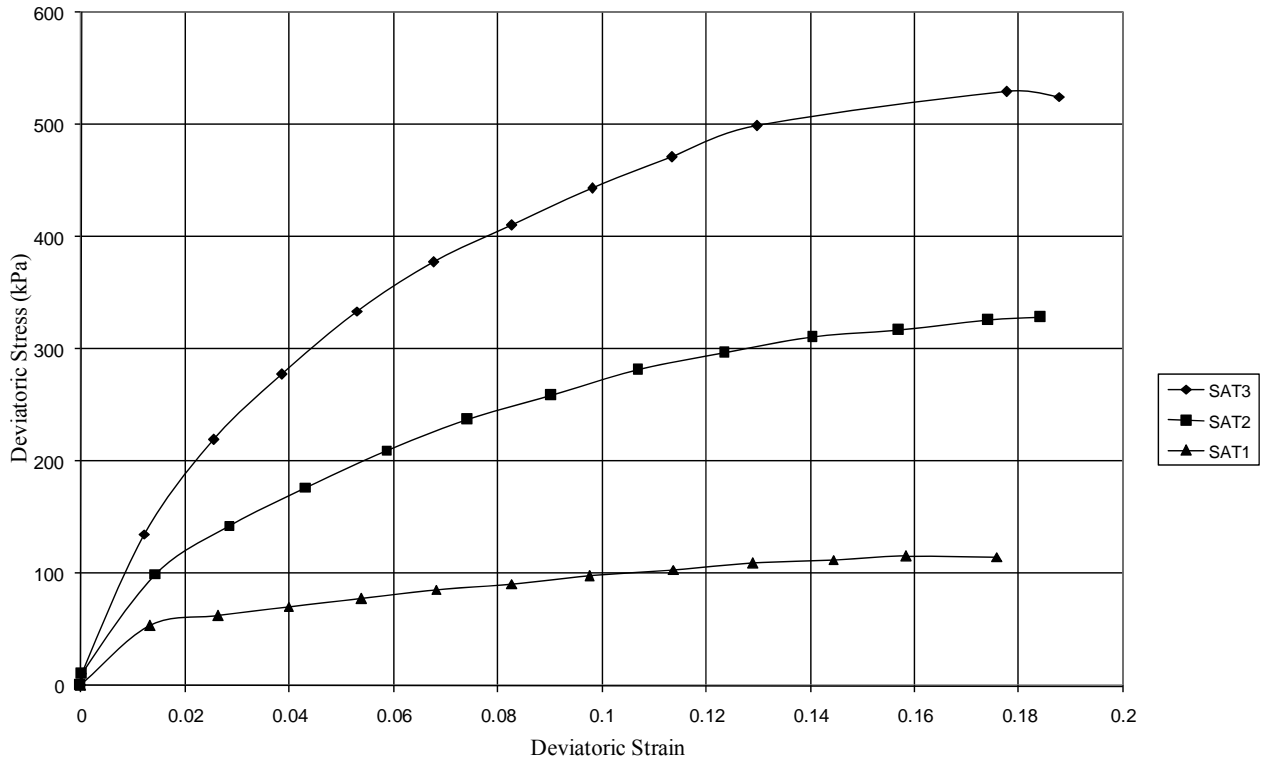

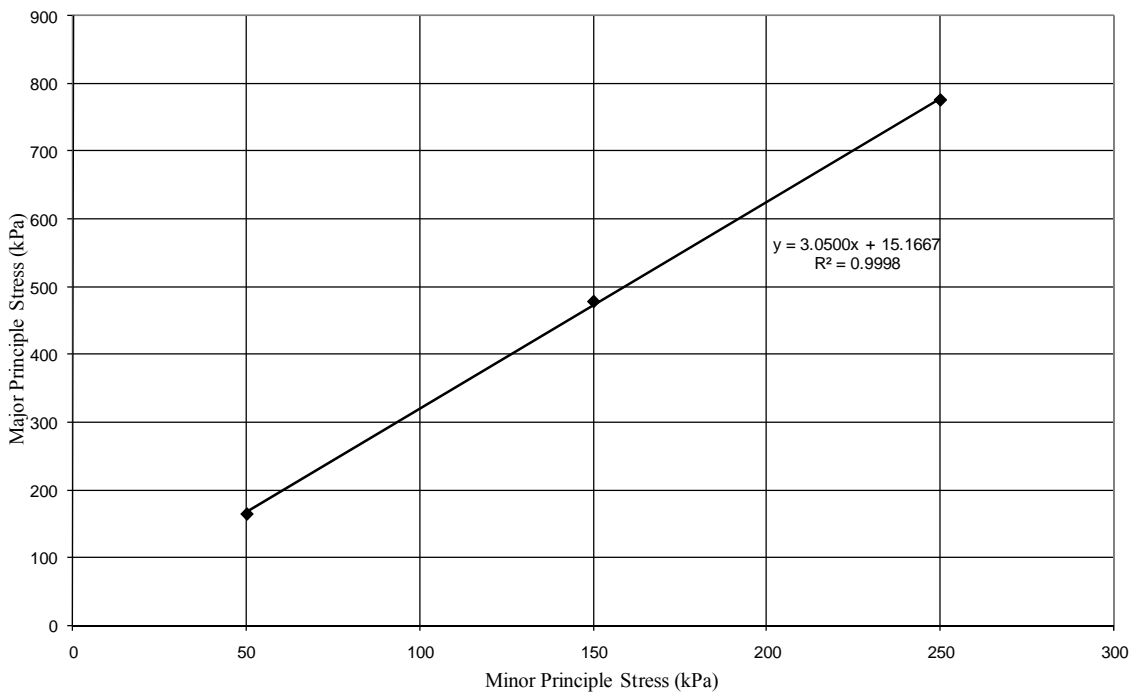Fig. 7. Deviatoric stress-strain curve for saturated specimens

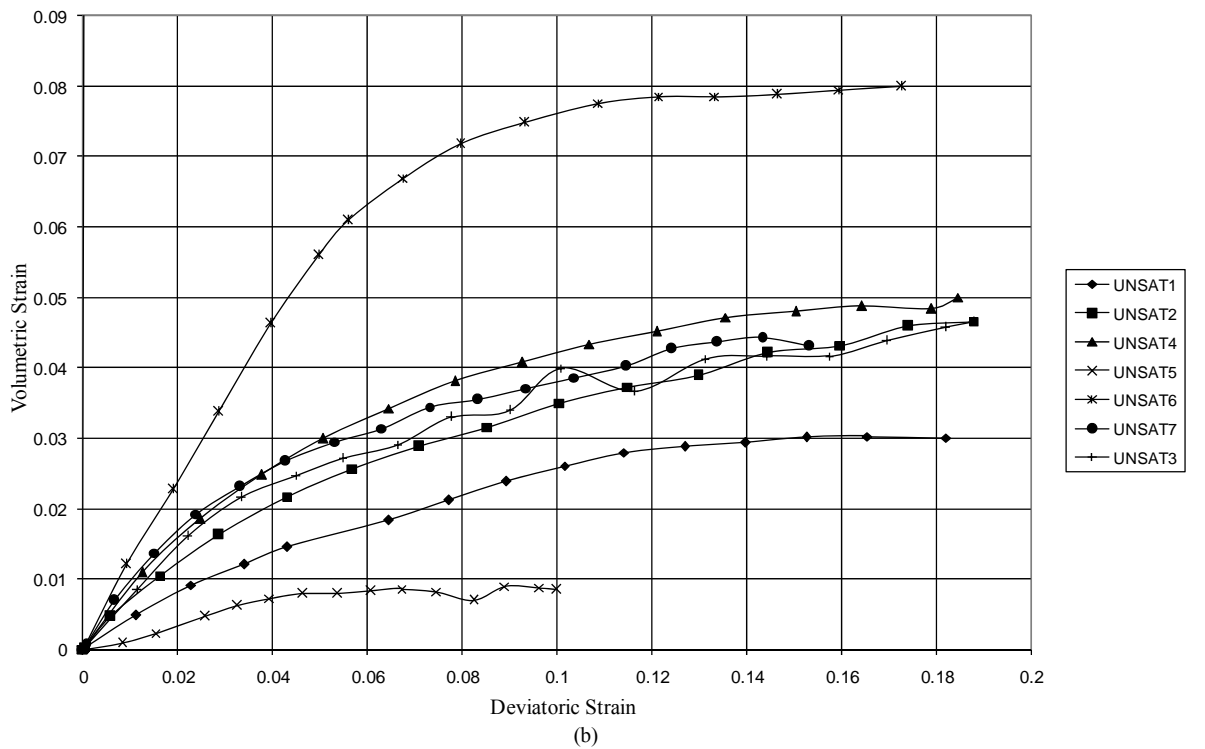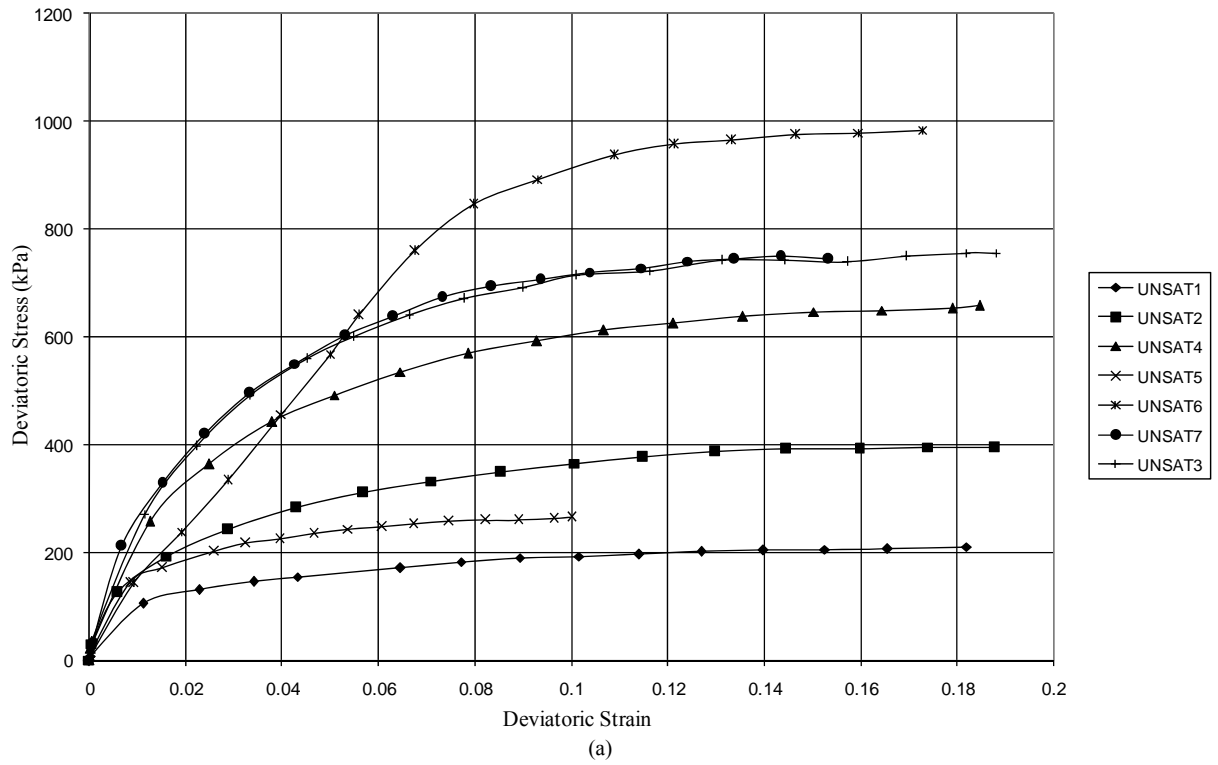Fig. 8. Mohr-coulomb failure criteria for saturated tests

(a)

(b)

Fig. 9. Deviatoric stress and volume change versus deviatoric strain for unsaturated tests

A. Fazeli et al.

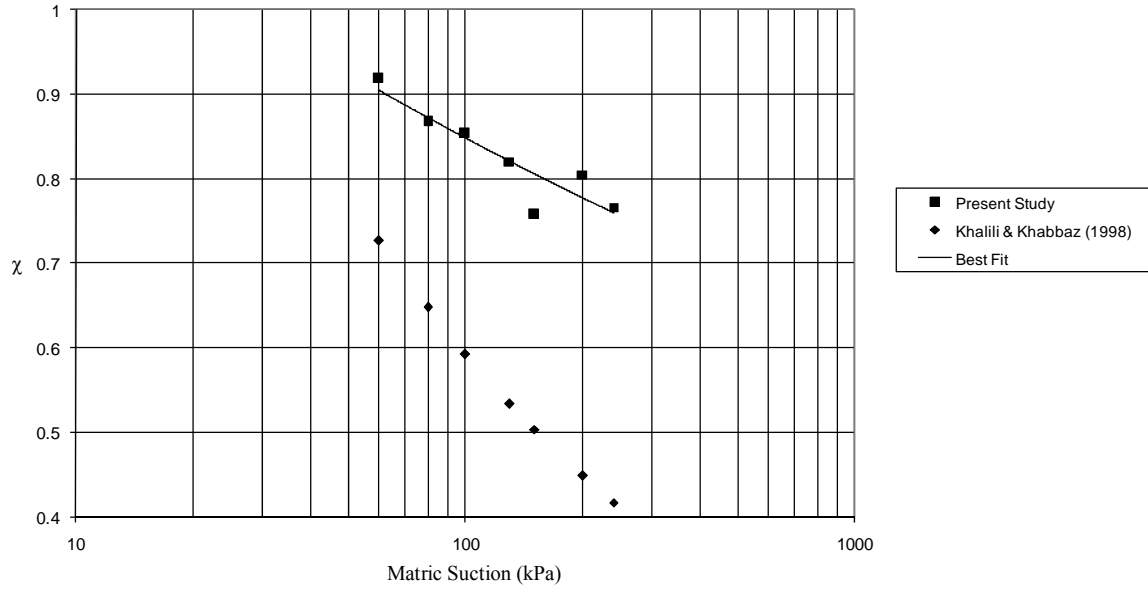
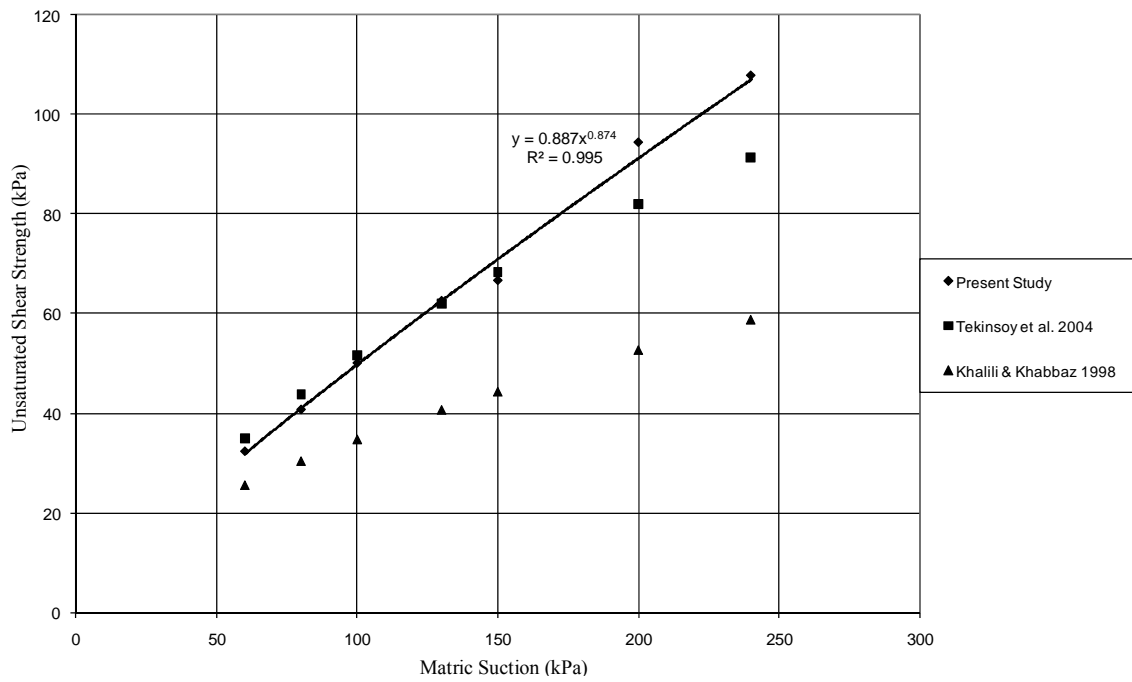Fig. 10. Variation of χ versus matric suction

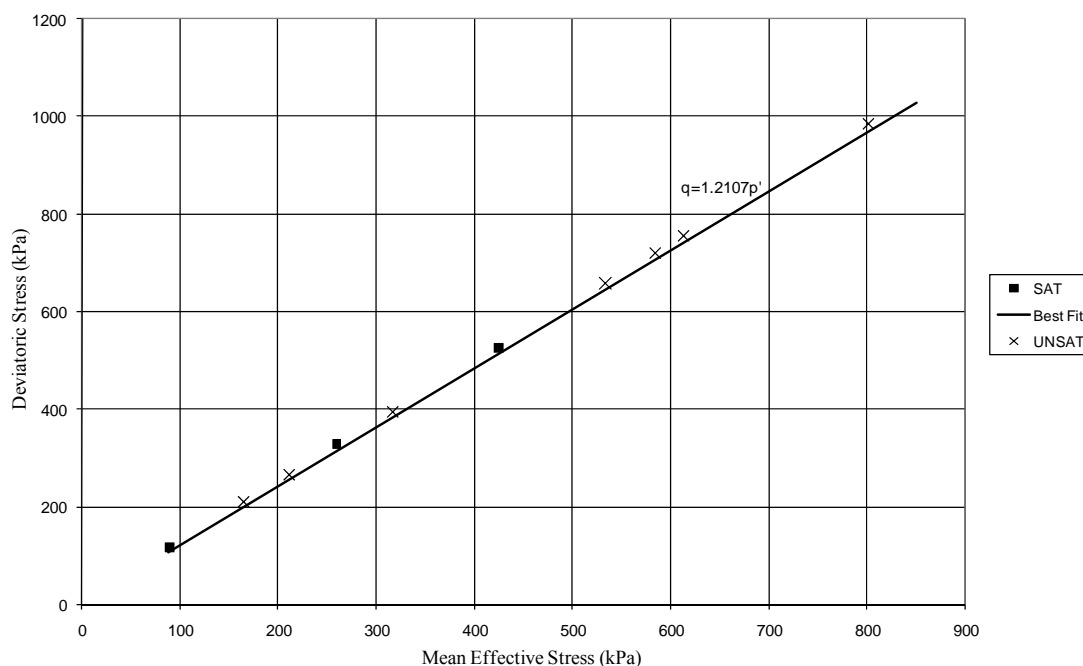Fig. 11. Variation of shear strength contributed to matric suction versus matric suction

Fig. 12. Variation of deviatoric stress versus mean effective stress for saturated and unsaturated tests

4. CONCLUSION

Shear strength of statically compacted samples of Shiraz silty clay was studied using saturated and unsaturated CD triaxial tests. The deviatoric stress was corrected considering the variation of sample average diameter during each test. Volume change and diameter measurements were determined using digital image processing. The effective friction angle and cohesion of Shiraz silty clay were determined as 30.4 degrees and 4.3 kPa, respectively, based on the results of tests on saturated specimens. An equation was obtained for the relationship between the shear strength parameter χ and the matric suction in Shiraz silty clay. The air entry value of the soil obtained from the above mentioned equation was very close to the value obtained from the pressure plate test. The main reason for the difference was considered to rise from the different values of mean net stress in these two different tests.

The relationship proposed by Tekinsoy et al. [16] predicts the shear strength contribution from matric suction, τ_{unsat}, for Shiraz silty clay with a higher precision compared to the relationship presented by Khalili and Khabbaz [10].

Furthermore, the unique linear relationship between the deviatoric stress and mean effective stress for all saturated and unsaturated tests indicates the validity of the effective stress principle in describing the shear strength of unsaturated soils for the range of suctions applied in this study.

REFERENCES

1. Aitchison, G. D. & Donald, I. B. (1956). Effective stresses in unsaturated soils. *Proceeding of the 2nd Australia– New Zealand Conference on Soil Mechanics and Foundation Engineering*, Christchurch, New Zealand, 192-199, Technical Publication Ltd.

2. Bishop, A. W. (1959). The principle of effective stress. *Teknisk Ukeblad*, Vol. 106, No. 39, pp. 859-863.

3. Wheeler, S. J. & Sivakumar, V. (1995). An elastoplastic critical state framework for unsaturated soil. *Geotechnique*, Vol. 45, No. 1, pp. 35-53.

4. Loret, B. & Khalili, N. (2002). An effective stress elastic-plastic model for unsaturated porous media. *Mechanics of Material*, Vol. 34, No. 2, pp. 97-116.

5. Gan, K. M., Fredlund, D. G. & Rahardjo, H. (1988). Determination of the shear strength parameters of an unsaturated soil using the direct shear test. *Canadian Geotechnical Journal*, Vol. 25, No. 3, pp. 500-510.

6. Rahardjo, H. & Fredlund, D. G. (1996). Consolidation apparatus for testing unsaturated soils. *Geotechnical Testing Journal*, Vol. 19, No. 4, pp. 341-350.

7. Rahnema, A., Habibagahi, G. & Ghahramani, A. (2003). A new simple shear apparatus for testing unsaturated soils. *Iranian Journal of Science and Technology, Transaction B, Engineering*, Vol. 27, No. 1, pp. 73-80.

8. Lamborn, M. J. (1986). A micromechanical approach to modeling partly saturated soils. *M.Sc. Thesis*, Texas A & M University, Texas, USA.

9. Vanapalli, S. K., Fredlund, D. G., Pufahl, D. E. & Clifton, A. W. (1996). Model for the prediction of shear strength with respect to soil suction. *Canadian Geotechnical Journal*, Vol. 33, pp. 379-392.

10. Khalili, N. & Khabbaz, M. H. (1998). A unique relationship for χ for the determination of the shear strength of unsaturated soil. *Geotechnique*, Vol. 48, No. 5, pp. 681-687.

11. Xu, Y. F. (2004). Fractal approach to unsaturated shear strength. *ASCE Journal of Geotechnical and Geoenvironmental Engineering*, Vol. 130, No. 3, pp. 264-273.

12. Nuth, M. & Laloui, L. (2008). Effective stress concept in unsaturated soils: clarification and validation of a unified framework. *Int. J. Numer. Anal. Meth. Geomech.*, Vol. 32, pp. 771-801.

13. Fredlund, D. G., Morgenstern, N. R. & Widger R. S. (1978). The shear strength of unsaturated soils. *Canadian Geotechnical Journal*, Vol. 15, No. 3, pp. 313-321.

14. Escario, V. & Juca, J. F. T. (1989). Strength and deformation of partly saturated soils. *Proceeding of the 12th International Conference on Soil Mechanics and Foundation Engineering*, Rio de Janeiro, Vol. 1, pp. 43-46.

15. Garven, E. A. & Vanapalli, S. K. (2006). Evaluation of empirical procedures for predicting the shear strength of unsaturated soils. *Proceeding of the International Conference on Unsaturated Soils*, Balkema.

16. Tekinsoy, M. A., Kayadelen, C., Keskin, M. S. & Soylemez, M. (2004). An equation for predicting shear strength envelope with respect to matric suction. *Computer and Geotechnics*, Vol. 31, No. 7, pp. 589-593.

17. Head, K. H. (1986). *Manual of soil laboratory testing*. Pentech Press, London.

18. Cole, D. M. (1978). A technique for measuring radial deformation during repeated load triaxial testing. *Canadian Geotechnical Journal*, Vol. 15, pp. 426-429.

19. Khan, M. H. & Hoag, D. L. (1979). A noncontacting transducer for measurement of lateral strain. *Canadian Geotechnical Journal*, Vol. 16, pp. 409-411.

20. Wheeler, S. J. & Sivakumar, V. (1992). Critical state concepts for unsaturated soil. *Proceeding of 7th International Conference on Expansive Soils*. Dallas, Tx, pp. 167-172.

21. Macari, E. J., Parker, J. K. & Costes, N. C. (1997). Measurement of volume changes in triaxial tests using digital image techniques. *Geotechnical Testing Journal*, Vol. 20, No. 1, pp. 103-109.

22. Geiser, F., Laloui, L. & Vulliet, L. (2000). On the volume measurement in unsaturated triaxial test. *Proceeding of Unsaturated Soils for Asia*, Singapore, pp. 669-674, Balkema.

23. Rifa'i, A., Laloui, L. & Vulliet, L. (2002). Volume measurement in unsaturated triaxial test using liquid variation and image processing. *Proceeding of the 3rd International Conference on Unsaturated Soils*, Editors: Juca, de Campos & Marinho, Rio de Janeiro, Brazil, Vol. 2, pp. 441-446, Balkema.

24. Elkady, T. Y., Houston, W. N. & Houston, S. L. (2002). Calibrated image processing for unsaturated soils testing. *Proceeding of the 3rd International Conference on Unsaturated Soils, Editors: Juca, de Campos & Marinho, Rio de Janeiro*, Brazil, Vol. 2, pp. 447-451, Balkema.

25. Oren, A. H., Onal, O., Ozden, G. & Kaya, A. (2006). Nondestructive evaluation of volumetric shrinkage of compacted mixtures using digital image analysis. *Engineering Geology*, Vol. 85, pp. 239-250.

26. Gachet, P., Geiser, F., Laloui, L. & Vulliet, L. (2007). Automated digital image processing for volume change measurement in triaxial cells. *Geotechnical Testing Journal*, Vol. 30, No. 2, pp. 98-103.

27. ASTM D-6836, (2003). Standard test method for soil water characteristic curve for desorption using pressure extractor. American Society for Testing and Material, Philadelphia, USA.

28. Rahardjo, H., Heng, O. B. & Choon, L. E. (2004). Shear strength of compacted residual soil from consolidated drained and constant water content tests. *Canadian Geotechnical Journal*, Vol. 41, pp. 421-436.

29. Bishop, A. W. & Wesley, L. D. (1975). A hydraulic triaxial apparatus for controlled stress path testing. *Geotechnique*, Vol. 25, No. 4, pp. 657-670.

30. Toll, D. G. (1993). *A computer control system for stress path triaxial testing. In developments in civil and construction engineering computing*. Editor: Topping, B.H.V., Edinburgh, UK, pp. 107–113, Civil-Comp Press.

31. Fredlund, D. G. & Rahardjo, H. (1993). *Soil mechanics for unsaturated soils*. John Wiley and Sons, Inc.

32. Mathworks, Inc. (2004). MATLAB User Guide. Version 7.

33. Otsu, N. (1979). A threshold selection method from gray-level histograms. *IEEE Transactions on Systems, Man, and Cybernetics*, Vol. 9, No. 1, pp. 62-66.